Effect of Electrode Route Motion on Electrode Wear in EDM Machining of Mold Steel

Dyi-Cheng Chen, Yi-Kai Wang & Geng-Fu Lin

Arabian Journal for Science and Engineering

ISSN 1319-8025
Volume 38
Number 10

Arab J Sci Eng (2013) 38:2793-2800
DOI 10.1007/s13369-012-0486-9

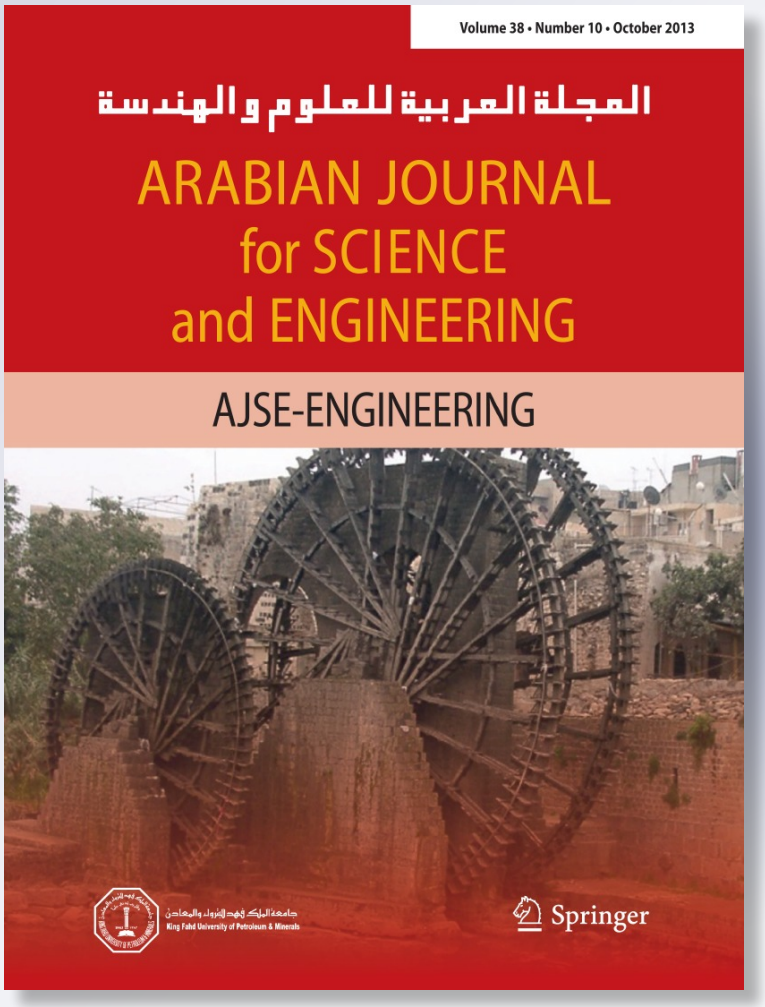

Springer

Arab J Sci Eng (2013) 38:2793–2800
DOI 10.1007/s13369-012-0486-9

RESEARCH ARTICLE - MECHANICAL ENGINEERING

Effect of Electrode Route Motion on Electrode Wear in EDM Machining of Mold Steel

Dyi-Cheng Chen · Yi-Kai Wang · Geng-Fu Lin

Received: 20 August 2011 / Accepted: 12 January 2012 / Published online: 9 January 2013

Abstract In the electrical discharge machining (EDM) of deep holes, electrode wear may cause the dimensions of the finished holes to deviate from their design values. In practice, the extent of the electrode wear and the surface roughness of the machined holes depend not only on the EDM machining parameters (e.g., the pulse duration, the pulse current, and so on), but also on the electrode route motion. Accordingly, the present study performs an experimental investigation into the effects of three different electrode routes (straight dip, spiral attack hole, and awl free expand hole) on the electrode wear and surface roughness of the machined holes in the EDM machining of PDS5A and PDS-1 mold steel, respectively. Overall, the experimental results show that of the three electrode route motions, the awl free expand hole motion results in a more uniform wear of the electrode and a lower surface roughness of the machined hole.

Keywords Electrical discharge machining · Electrode route motion · Electrode wear

D.-C. Chen (✉) · Y.-K. Wang · G.-F. Lin
Department of Industrial Education and Technology,
National Changhua University of Education,
Changhua 500, Taiwan, ROC
e-mail: dcchen@cc.ncue.edu.tw

الخلاصة

في آلات التفريغ الكهربائية (EDM) ذات الثقوب العميقه قد يسبب تآكل القطب إلى انحراف قياسات الثقوب النهائية من قيمها التصميمية. ومن الناحية العملية فإن مدى تآكل القطب وخشونة السطح للثقوب لا تعتمد فقط على معاملات تصنيع الآلات (مثلاً: مدى النبض، وتيار النبض، وما إلى ذلك) ولكن أيضا على حركة طريق القطب. وبناء على ذلك تؤدي هذه الدراسة إلى التحقق المخبري من تأثير ثلاث طرق أقطاب مختلفة (الـ DIP المستقيم، والثقب الحلزوني، ومعزز ثقب التمدد الحر) وذلك لتآكل القطب وخشونة السطح للثقوب النهائية في تشكيل EDM وذلك لقالب حديدي من PDS5A و PDS-1 على التوالي. وبعامة فقد أظهرت النتائج لحركات الأقطاب الثلاثة، إن ثقب التمدد الحر لديه تآكل منتظم أكثر للقطب وأقل خشونة سطح لتشكيل الثقب.

1 Introduction

Electrical discharge machining (EDM) is a non-traditional manufacturing process in which material is removed from the workpiece by means of a series of electrical discharges between two electrodes (i.e., the tool and the workpiece) separated by a dielectric fluid. Luis et al. [1] examined the material removal rate (MRR) and electrode wear rate (EWR) in the EDM of siliconized or reaction-bonded silicon carbide (SiSiC). Marafona [2] showed that the carbon layer formed on the electrode in the die-sinking EDM process is beneficial in reducing the electrode wear ratio (EWR). Kunieda and Kobayashi [3] performed spectroscopic measurements of the vapor density of the electrode material in EDM arc plasma. The results showed that the density of the copper vapor evaporated from the electrode surface reduced as the thickness of the carbon layer deposited on the tool increased; indicating that the carbon layer provided an effective reduction in the electrode wear. Zhao et al. [4] utilized a selective laser sintering (SLS) technique to fabricate EDM electrodes, and showed that by optimizing the SLS parameters, the

machining performance of the electrode approached that of solid copper electrodes.

Kunieda and Kameyama [5] showed that the electrode wear in the EDM process could be reduced by applying a relative sliding motion between the tool and the workpiece. Mohri et al. [6] observed the time-dependence of the electrode shape in EDM via on-the-machine measurements, and showed that the electrode wears at the edge portion during the initial stage of machining and then wears in the longitudinal direction of the flat portion as machining continues. Lin et al. [7] utilized the Taguchi design method and fuzzy logic to optimize the EDM parameters in such a way as to minimize the EWR whilst simultaneously maximizing the MRR. Chen et al. [8] investigated the effects of kerosene and distilled water dielectrics on the EDM characteristics of titanium alloy (Ti-6Al-4V). The results showed that distilled water results in both a lower EWR and a higher MRR than kerosene. Mahardika et al. [9] proposed a method for determining the ease of machining of a workpiece using EDM based on the thermal conductivity, melting point and electrical resistivity of the workpiece material. Rhoney et al. [10] used stereographic scanning electron microscopy (SEM) to investigate the wear mechanism in the wire EDM truing of metal bond diamond wheels for ceramic grinding. The SEM observations showed that the EDM process left more than half the diamond height exposed, thereby weakening the bond between the diamond and the wheel and leading to diamond fracture under even light grinding conditions. Wang and Lin [11] utilized the Taguchi design method to optimize the polarity, peak current, pulse duration, duty factor, rotary electrode rotational speed, and gap-load voltage parameters of the EDM process in such a way as to maximize the MRR of sintered W/Cu composites whilst simultaneously minimizing the EWR and surface roughness of the machined component.

In general, the studies described above focus primarily on the effects of the EDM parameters on the electrode wear rate. However, in practice, both the electrode wear rate and the surface roughness of the machined workpiece are also affected by the electrode route motion. Accordingly, the present study performs an experimental investigation into the effects of three different electrode route motions (straight dip, spiral attack hole, and awl free expand hole) on the electrode wear and surface roughness characteristics in the EDM processing of mold steel.

2 Experimental Studies

2.1 Experimental Materials

The EDM machining trials were conducted using two different mold steels, namely, PDS5A (AISI: P20) and PDS-1 (JIS: S55C). In both cases, machining was performed using brass electrodes. The element compositions of the mold steel workpieces and the brass electrodes are shown in Table 1. Two different types of electrode were prepared using a milling machine, namely, a 4.8 mm square electrode (designated as the rough electrode) and a 4.9 mm square electrode (designated as the refined electrode). Prior to the EDM trials, the electrode surfaces were wiped with copper oil in order to remove any traces of the milling cutter. Figure 1 presents a photograph of the electrodes and the two workpiece materials.

Table 1 Element compositions of mold steel workpieces and brass electrodes

PDS5A (quite specification)				
Special steel		AISI		
PDS5A		P20		
Essential composition: %				
C	Mn	Cr	Mo	Special elements
0.25–0.35	0.95–1.15	2.00–3.00	0.30–0.50	
PDS-1 (quite specification)				
Special steel		JIS G4051		AISI
PDS-1		S55C		1055
Essential composition: %				
C	Si	Mn	P	S
0.52–0.60	0.200.35	0.60–0.90	≤0.040	≤0.050
Brass essential composition				
Alloy	Cu	Pb	Fe	Zn
CuZn40	59–62	<0.10	<0.07	others

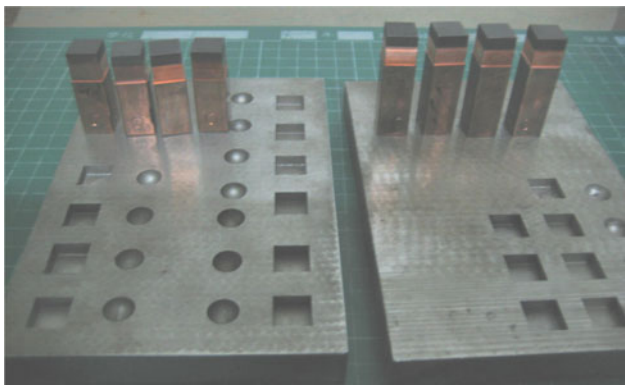

Fig. 1 Mold steel workpieces and brass electrodes

2.2 Experimental Facilities and Process

2.2.1 Experimental Facilities

(1) A milling machine (to prepare the electrodes), (2) an S505A numerical control EDM system (Fig. 2), and (3) a Brown and Sharpe photographic-type contactless precision measurement system (Fig. 3).

Fig. 2 S505A EDM system

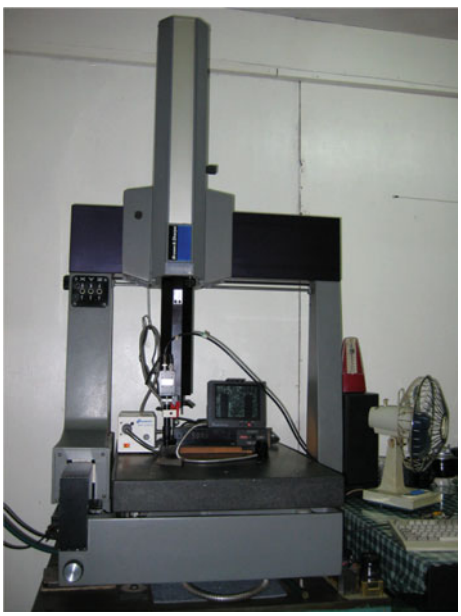

Fig. 3 Photographic-type contactless measurement system

2.2.2 *Experiment Process*

For each workpiece material, the rough electrode was used to machine 4.8 mm blind holes using three different electrode route motions, namely, straight dip (G111), spiral attack hole (G133), and awl free expand hole (G135). Thereafter, the three holes were finished using the 4.9 mm refined electrode with the G111, G133 and G135 electrode route motions, respectively. The experimental program and the corresponding electrode/workpiece designations are summarized in Table 2. As shown in the rightmost column of the

Table 2 Summary of experimental program and designations

EDM steel	Electrode shape	No.	Process method	Using parameter
Mold steel PDS5A	Square	P11	G111 rough finish	A901 code
			G111 precision finish	A900 code
		P12	G133 rough finish	A901 code
			G133 precision finish	A900 code
		P13	G135 rough finish	A901 code
			G135 precision finish	A900 code
Mold steel PDS-1	Square	D11	G111 rough finish	A901 code
			G111 precision finish	A900 code
		D12	G133 rough finish	A901 code
			G133 precision finish	A900 code
		D13	G135 rough finish	A901 code
			G135 precision finish	A900 code

Table 3 EDM parameters [12]

Code	parameter	MD	VP	IH	IL	ON	WR	OF	SV	SK	SN	JD
A900	09303	3	4	2	13	30	2	33	20	3	5	4
	09202	1	4	2	3	5	0	18	70	2	5	2
A901	09373	3	2	2	25	45	2	45	20	4	7	2
	09363	3	2	2	22	30	2	35	20	4	5	2
	09343	3	2	2	20	15	2	25	20	3	5	2
	09323	3	2	2	17	10	2	20	20	3	5	2

Table 4 Electrode route motions [CNC EDM operation catalogue]

Syntax	function	Schematic of route
G111	Straight dip process	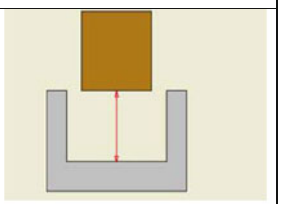
G133	Spiral attack hole process	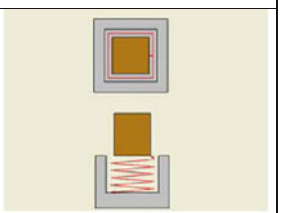
G135	Awl free expand hole process	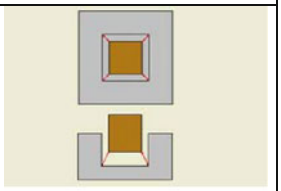

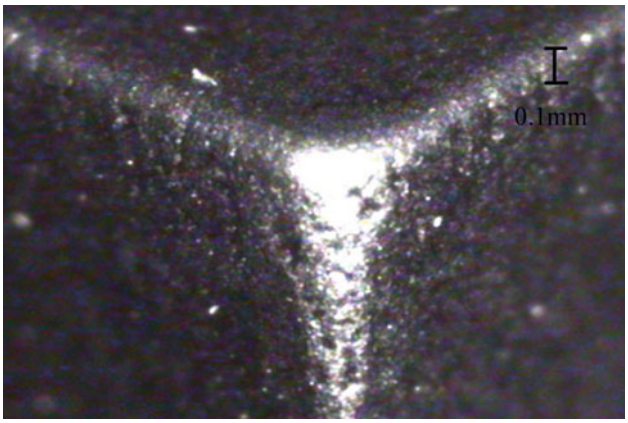

Fig. 4 Corner region of P11 electrode

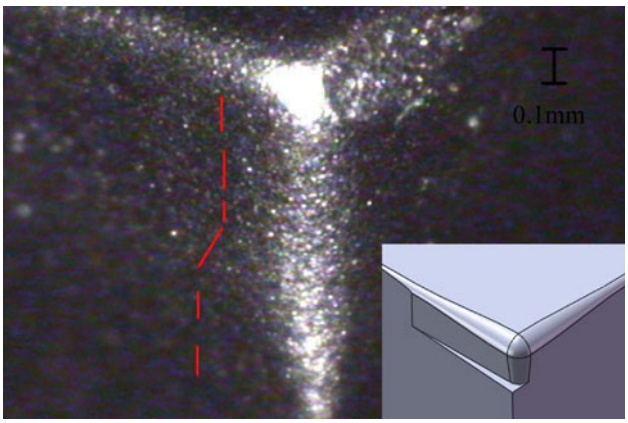

Fig. 5 Corner region of P12 electrode

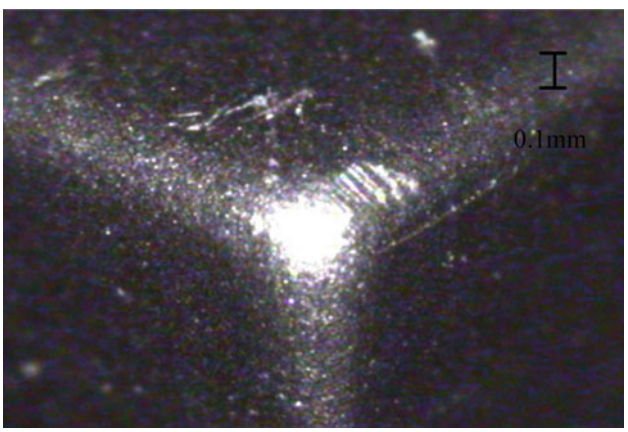

Fig. 6 Corner region of P13 electrode

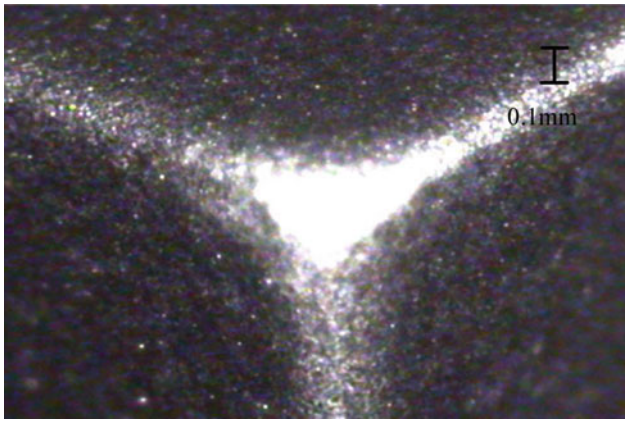

Fig. 7 Corner region of D11 electrode

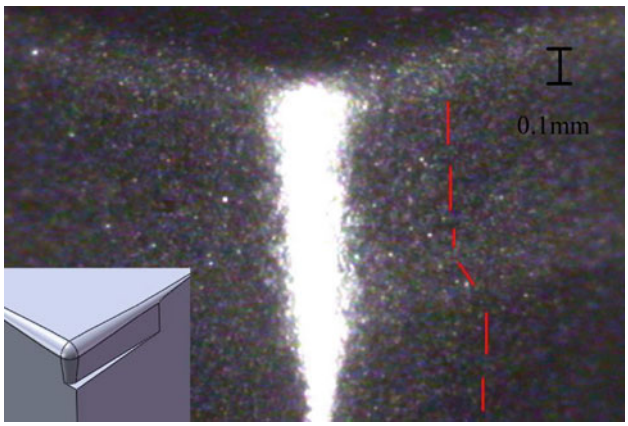

Fig. 8 Corner region of D12 electrode

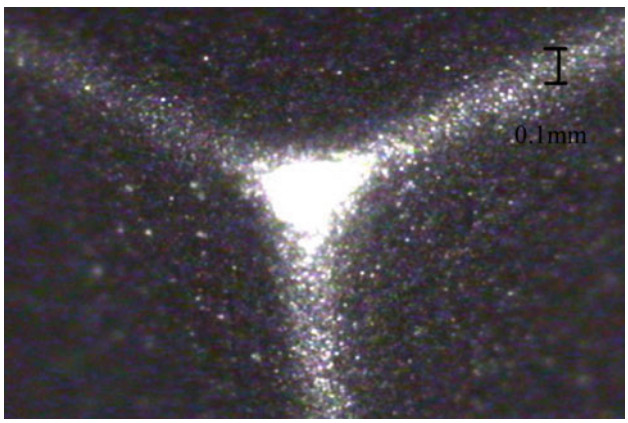

Fig. 9 Corner region of D13 electrode

table, the rough finish machining operations were performed using the A901 parameter set (Table 3 [CNC EDM operation catalogue]), while the precision finish machining operations were performed using the A900 parameter set. The parameters included: MD (Machining Mode), VP (Voltage and Polarity), IH (High Voltage Current), IL (Low Voltage Current), ON (On Time), OF (Off Time), SV (Servo Gap), SK (Servo Gain), SN (Servo Noise Rejection) and JD (Jump Down). The dielectric fluid used 50 viscosity S.S.U. hydrocarbon oil. Machining time is 30 min for rough finish and 90 min for precision finish. The three electrode route motions are illustrated schematically in Table 4 [12]. The motions include straight dip process (G111), spiral attack hole process (G133) and awl free expand hole process (G135). Awl free expand hole process induced four corner for electrode route motion.

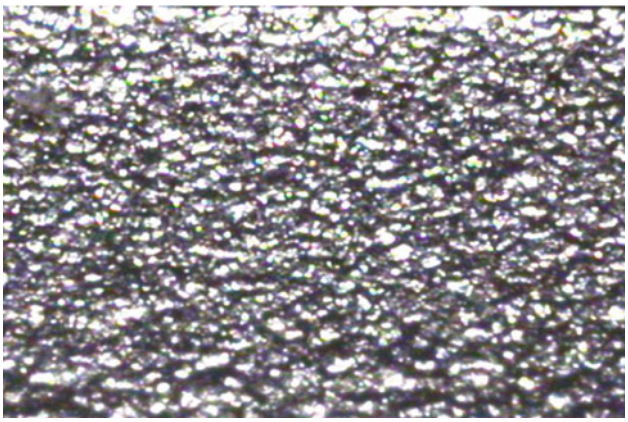

Fig. 10 Inner wall of hole processed using P11 electrode

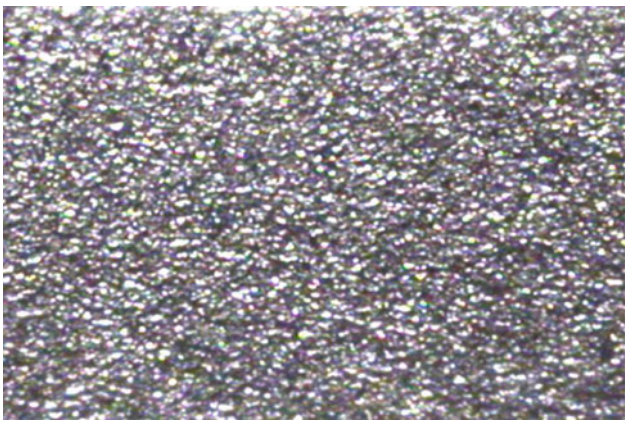

Fig. 11 Inner wall of hole processed using P12 electrode

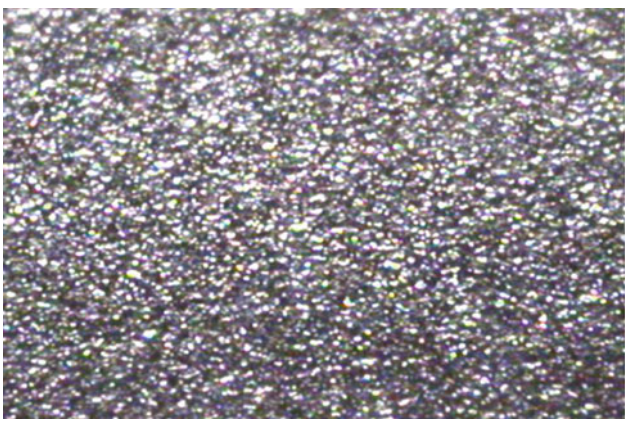

Fig. 12 Inner wall of hole processed using P13 electrode

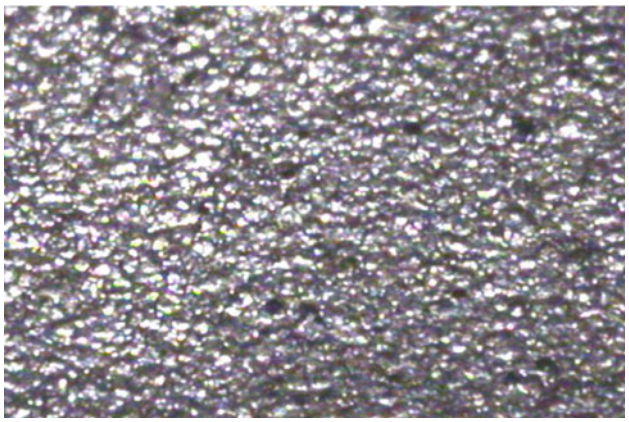

Fig. 13 Inner wall of hole processed using D11 electrode

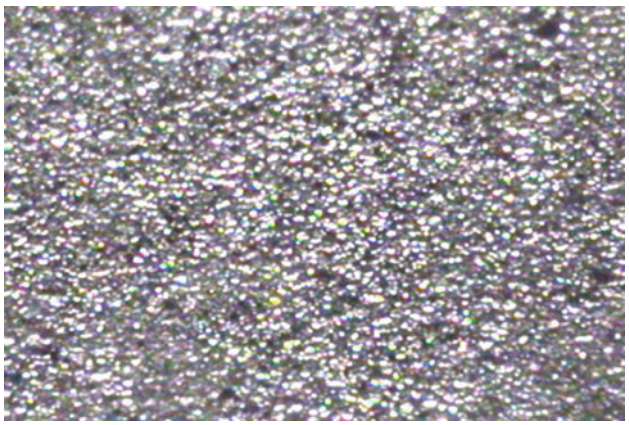

Fig. 14 Inner wall of hole processed using D12 electrode

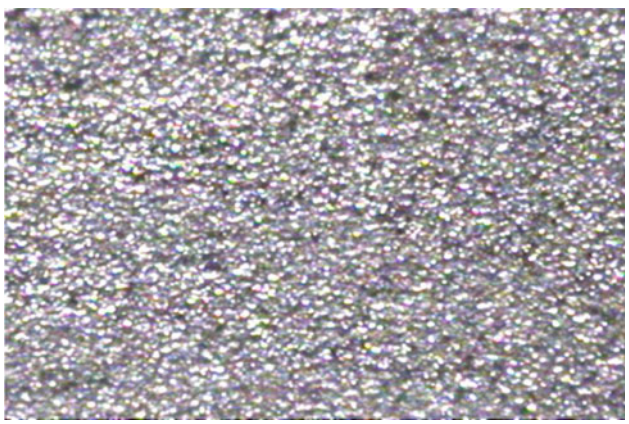

Fig. 15 Inner wall of hole processed using D13 electrode

3 Results and Analysis

3.1 Electrode Wear

Figures 4, 5, 6, 7, 8, 9 present photographs of the six electrodes (i.e., P11–P13 and D11–D13, see Table 2) following the machining process. It is observed that in the machining trials performed using the straight dip route motion (G111), the electrodes exhibit significant localized wear in the corner region (Figs. 4, 7). Similarly, for the machining trials performed using the spiral attack hole route motion (G133), the electrodes exhibit a step-like wear of the side contact surface (Figs. 5, 8). However, in the machining trials performed using the awl free expand hole process (G135), the electrodes exhibit a uniform wear in the corner region (Figs. 6, 9).

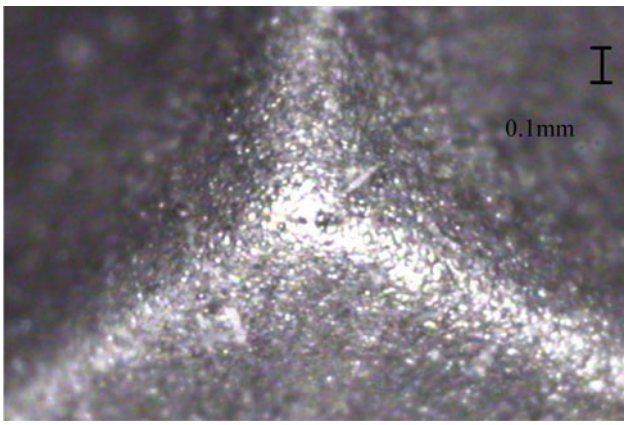

Fig. 16 Corner of hole processed using P11 electrode

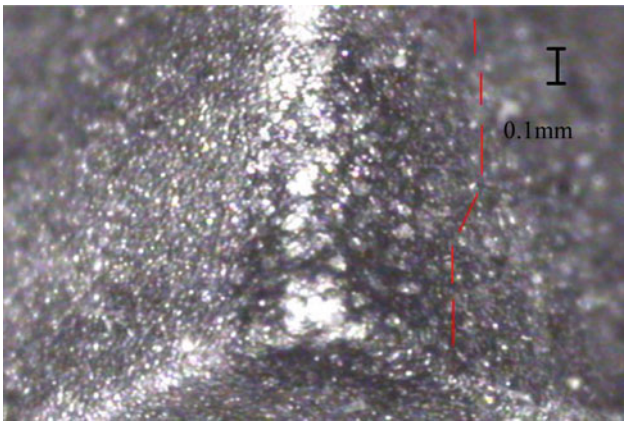

Fig. 17 Corner of hole processed using P12 electrode

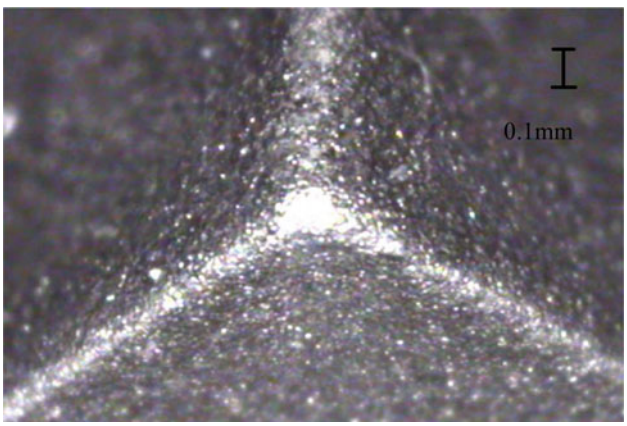

Fig. 18 Corner of hole processed using P13 electrode

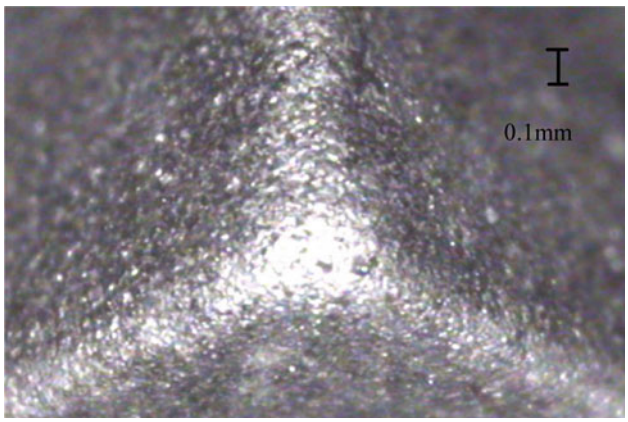

Fig. 19 Corner of hole processed using D11 electrode

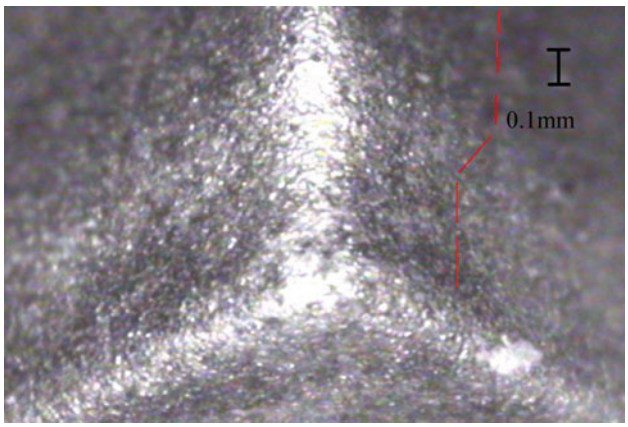

Fig. 20 Corner of hole processed using D12 electrode

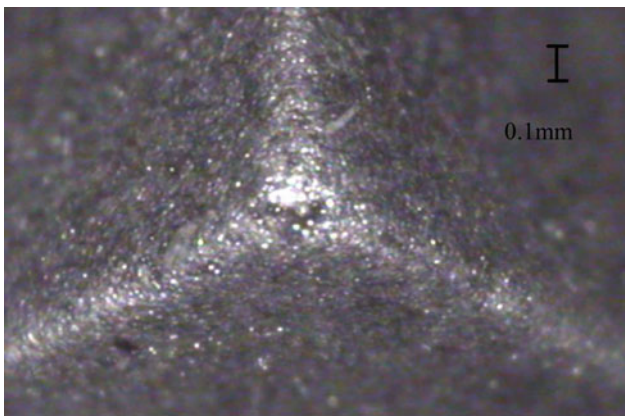

Fig. 21 Corner of hole processed using D13 electrode

3.2 Workpiece Surface Roughness

For the PDS5A mold steel, the average surface roughness was found to be Ra = 2.023 μm when using the G111 electrode route motion, Ra = 1.37 μm when using the G133 route motion, and Ra = 1.337 μm when using the G135 route motion. Similarly, for the PDS-1 workpiece, the average surface roughness was found to be Ra = 1.862 μm, Ra = 1.435 μm and Ra = 1.423 μm, when using the G111, G133 and G135 route motions, respectively. In other words, for both mold steels, the G135 (awl free hole expand) electrode route motion yields the lowest surface roughness.

Figures 10, 11, 12, 13, 14, 15 present photographs of the inner wall of the holes machined in the PDS5A and PDS-1

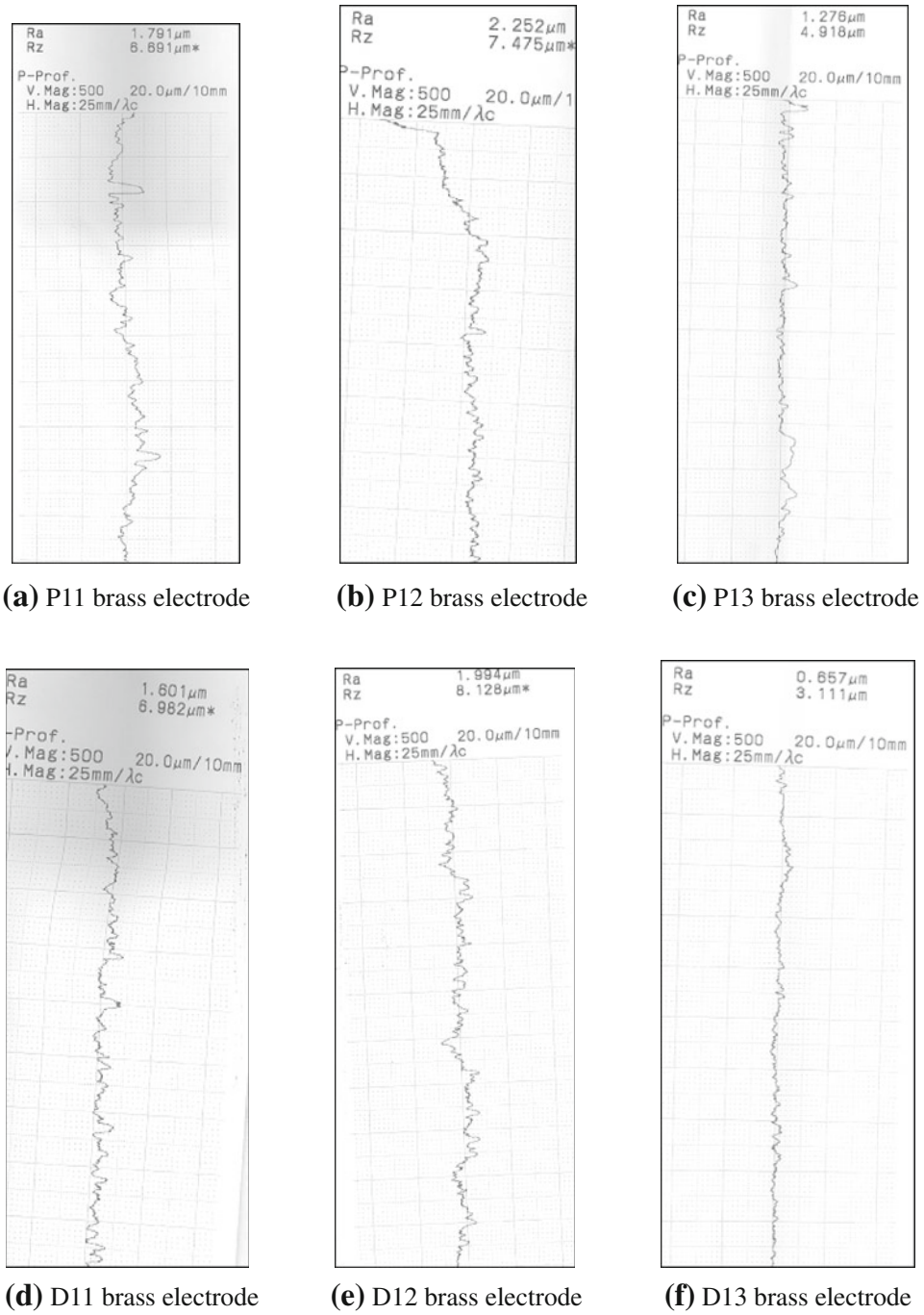

(a) P11 brass electrode **(b)** P12 brass electrode **(c)** P13 brass electrode

(d) D11 brass electrode **(e)** D12 brass electrode **(f)** D13 brass electrode

Fig. 22 Surface roughness of hole processed using P11, P12, P13, D11, D12, D13 brass electrode

workpieces using the three different electrode route motions. Meanwhile, Figs. 16, 17, 18, 19, 20, 21 present enlarged photographs of the corner region of each hole. Figures 12 and 15 confirm that the awl free hole expand route motion yields a qualitative improvement in the surface roughness of the machined hole. In addition, the awl free hole expand route motion results in a clearly defined corner feature at the base of the hole (Figs. 18, 21). In contrast, the straight dip process yields a more imprecise corner feature (Figs. 16, 19), while the spiral attack hole route motion results in the formation of a step-like feature in the wall surface (Figs. 17, 20).

Figure 22 present photographs of surface roughness of brass electrode in the PDS5A and PDS-1 workpieces using the three different electrode route motions. It shows the surface roughness including P11 brass electrode (Ra = 1.791 um, Rz = 6.691 um), P12 brass electrode (Ra = 2.252 um, Rz = 7.475 um), P13 brass electrode

(Ra = 1.276 um, Rz = 4.918 um), D11 brass electrode (Ra = 1.601 um, Rz = 6.982 um), D12 brass electrode (Ra = 1.994 um, Rz = 8.128 um), D13 brass electrode (Ra = 0.657 um, Rz = 3.111 um). It can be seem that P12 brass electrode has larger surface roughness, and D13 brass electrode has smaller surface roughness.

4 Conclusions

This study has investigated the effect of the EDM electrode route motion on the electrode wear and surface roughness characteristics of PDS5A and PDS-1 mold steel workpieces. The motions include straight dip process (G111), spiral attack hole process (G133) and awl free expand hole process (G135). Machining time is 30 min for rough finish and 90 min for precision finish. The major findings of this study can be summarized as follows: (1) the awl free expand hole route motion (G135) yields a more uniform wear of the electrode than the straight dip route motion (G111) or spiral attack hole route motion (G133). (2) The awl free expand hole route motion results in a lower surface roughness of the machined component than the straight dip route motion or spiral attack hole route motion.

Acknowledgments The authors gratefully acknowledge the support provided to this study by CHEN GEM TECHNOLOGY CO., LTD, Taiwan.

References

1. Luis, C.J.; Puertas, I.; Villa, G.: Material removal rate and electrode wear study on the EDM of silicon carbide. J. Mater. Process. Technol. **164**–**165**, 889–896 (2005)
2. Marafona, J.: Black layer characterization and electrode wear ratio in electrical discharge machining (EDM). J. Mater. Process. Technol. **184**, 27–31 (2007)
3. Kunieda, M.; Kobayashi, T.: Clarifying mechanism of determining tool electrode wear ratio in EDM using spectroscopic measurement of vapor density. J. Mater. Process. Technol. **149**, 284–288 (2004)
4. Zhao, J.; Li, Y.; Zhang, J.; Yu, C.; Zhang, Y.: Analysis of the wear characteristics of an EDM electrode made by selective laser sintering. J. Mater. Process. Technol. **138**, 475–478 (2003)
5. Kunieda, M.; Kameyama, A.: Study on decreasing tool wear in EDM due to arc spots sliding on electrodes. Precis. Eng. **34**, 546–553 (2010)
6. Mohri, N.; Suzuki, M.; Furuya, M.; Saito, N.; Kobayashi, A.: Electrode wear process in electrical discharge machining. Ann. CIRP. **44**(1), 165–168 (1995)
7. Lin, J.L.; Wang, K.S.; Yan, B.H.; Tarng, Y.S.: Optimization of the electrical discharge machining process based on the Taguchi method with fuzzy logics. J. Mater. Process. Technol. **102**, 48–55 (2000)
8. Chen, S.L.; Yan, B.H.; Huang, F.Y.: Influence of kerosene and distilled water as dielectrics on the electric discharge machining characteristics of Ti-6Al-4V. J. Mater. Process. Technol. **87**, 107–111 (1999)
9. Mahardika, M.; Tsujimoto, T.; Mitsui, K.: A new approach on the determination of ease of machining by edm processes. Int. J. Mach. Tools Manuf. **48**, 746–760 (2008)
10. Rhoney, B.K.; Shih, A.J.; Scattergood, R.O.; Ott, R.; McSpadden, S.B.: Wear mechanism of metal bond diamond wheels trued by wire electrical discharge machining. Wear **252**, 644–653 (2002)
11. Wang, C.C.; Lin, Y.C.: Feasibility study of electrical discharge machining for W/Cu composite. Int. J. Refract. Metals Hard Mater. **27**, 872–882 (2009)
12. CNC EDM operation catalogue Yihawjet Enterprises Co., LTD, Taiwan (2002)